22. *Arabidopsis* Biological Resource Center, 1735 Neil Avenue, Columbus, OH 43210.
23. J. Browse, N. Warwick, C. R. Somerville, C. R. Slack, *Biochem. J.* **235**, 25 (1986).
24. We thank E. Meyerowitz for RFLP markers and mapping information, E. Ward and G. Jen for the YAC library, K. Niyogi and G. Fink for the ASA2 marker, D. Murphy for the *B. napus* library, and E. Grill, B. Hauge, J. Schiefelbein, J. Martinez-Zapater, P. Gil, and K. Iba for advice. V.A., S.G., and B.L. were supported in part by fellowships from the European Molecular Biology Organization, National Institutes of Health, and the Natural Sciences and Engineering Research Council of Canada, respectively. Supported by grants DCB8916311 from the National Science Foundation and DE-FG02-90ER20021 from the U.S. Department of Energy to C.R.S., and a grant from Hoechst AG to H.M.G.

29 June 1992; accepted 15 September 1992

Dynamics of Ribozyme Binding of Substrate Revealed by Fluorescence-Detected Stopped-Flow Methods

Philip C. Bevilacqua, Ryszard Kierzek, Kenneth A. Johnson, Douglas H. Turner*

Fluorescence-detected stopped-flow and equilibrium methods have been used to study the mechanism for binding of pyrene (pyr)-labeled RNA oligomer substrates to the ribozyme (catalytic RNA) from *Tetrahymena thermophila*. The fluorescence of these substrates increases up to 25-fold on binding to the ribozyme. Stopped-flow experiments provide evidence that pyr experiences at least three different microenvironments during the binding process. A minimal mechanism is presented in which substrate initially base pairs to ribozyme and subsequently forms tertiary contacts in an RNA folding step. All four microscopic rate constants are measured for ribozyme binding of pyrCCUCU.

Recognition of the 5′ exon for splicing of the ribosomal RNA precursor of *T. thermophila* involves base pairing of the exon sequence CUCUCU with part of an intron internal guide sequence (IGS), GGAGGG, to give a helix designated P1 (*1*). This process can be mimicked with oligonucleotides and truncated forms of the intron (*2*, *3*). Tertiary interactions involving 2′-OH groups of substrate enhance this binding (*4*–*6*). Under conditions where all the ribozyme is active (*6*), we report transient kinetic studies indicating that tertiary contacts form after base pairing, and we provide the first rate constants for the dynamics of this RNA folding step (Fig. 1A).

Conjugation of pyrene to a 5′ amino-modified ribose (Fig. 1B) provides a probe of rapid binding steps (*7*). Binding of pyrCUCU, pyrCCUCU, pyrCUCUCU, and pyrCCCUCU to the L-21 Sca I form of the ribozyme from *T. thermophila* (*3*) increases pyr fluorescence by factors of 25, 21, 8, and 4, respectively (*8*), consistent with expectations based on three-dimensional models of the binding site (*9*). All four pyr-labeled substrates reacted in single turnover nucleotidyl transfer reactions with ^{32}P-labeled (p*) p*UCGA, suggesting that their fluorescence enhancement results from binding in the catalytic core (*10*). A typical reaction modeling the second step of splicing is

pyrCCUCU	+ p*UCGA	⇌
5′exon	3′splice	L-21
mimic	junction	Sca I
	pyrCCUCUA	+ p*UCG
	5′splice	3′end
	junction	of intron

Rapid mixing, stopped-flow experiments with L-21 Sca I and pyrCCUCU resulted in fast and slow rates for binding, $1/\tau_1$ and $1/\tau_2$, respectively (Fig. 2). Traces of fluorescence versus time after mixing were fit to a single or double exponential as appropriate. Plots of rates versus [pyrCCUCU] give a straight line fit for the faster rate and a hyperbolic fit for the slower rate (Fig. 3A). This is consistent with two-step binding in which base pairing of pyrCCUCU and the IGS to form P1 occurs in the first step and uptake of P1 occurs in the second step (Fig. 1A, Scheme I). The apparent enhancement of pyr fluorescence after tertiary folding is a unique observation for a nucleic acid (*7*). For Scheme I and substrate, S, in excess over L-21 Sca I (*11*)

$$\frac{1}{\tau_1} \approx k_1[S] + k_{-1} + k_2 + k_{-2} \quad (1)$$

$$\frac{1}{\tau_2} \approx \frac{k_1[S](k_2 + k_{-2}) + k_{-1}k_{-2}}{k_1[S] + k_{-1} + k_2 + k_{-2}} \quad (2)$$

where k_1, k_{-1}, k_2, and k_{-2} are the rate constants shown in Scheme I. Initial estimates of rate constants were obtained by fitting data in Fig. 3A to Eqs. 1 and 2. Rate constants were optimized by computer simulation of traces (Table 1) (*12*). The value

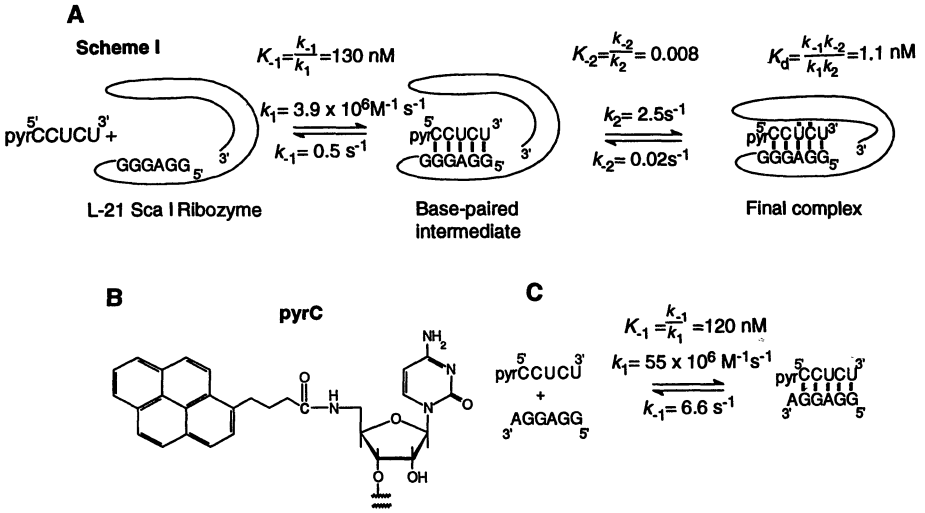

Fig. 1. (**A**) Minimal mechanism (Scheme I) consistent with all the data for all four 5′ exon mimics. The rate constants are for pyrCCUCU. The sketch of L-21 Sca I is not meant to give structural detail but to indicate that pyr is protected from solvent in both the intermediate and final state and less so as oligomer length increases. The sketch also depicts GGAGGG (IGS) as not completely accessible in the unbound L-21 Sca I. Lines indicate base pairing (*1*). Known tertiary hydrogen bonds involving 2′ OH groups of substrate (*5*, *6*) are indicated by bold dots. (**B**) Structure of the 5′ end of pyr-modified oligomers (pyrC). (**C**) Minimal mechanism for pyrCUCU and pyrCCUCU binding to the IGS mimic GGAGGA. The rate constants are for pyrCCUCU.

P. C. Bevilacqua and D. H. Turner, Department of Chemistry, University of Rochester, Rochester, NY 14627.
R. Kierzek, Institute of Bio-organic Chemistry, Polish Academy of Sciences, 60-704 Poznan, Noskowskiego 12/14, Poland.
K. A. Johnson, Department of Molecular and Cell Biology, Pennsylvania State University, Althouse Laboratory, University Park, PA 16802.
*To whom correspondence should be addressed.

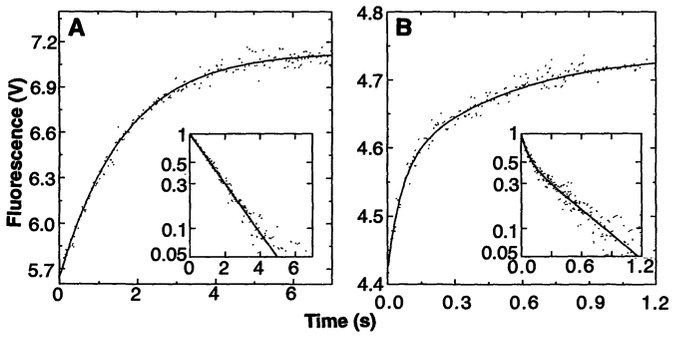

Fig. 2. Dependence of F on time after rapid mixing of equal volumes of pyrCCUCU and L-21 Sca I. Mixing was carried out in a KinTek stopped-flow apparatus with 1.5-ms mixing time (*30*). Final concentrations after mixing are 20 nM L-21 Sca I and (**A**) 0.2 μM pyrCCUCU or (**B**) 3.2 μM pyrCCUCU. (A) Data are fit to $F = F_\infty + F_2e^{-t/\tau_2}$, resulting in $1/\tau_2 = 0.60\ s^{-1}$. (B) Data are fit to $F = F_\infty + F_1e^{-t/\tau_1} + F_2e^{-t/\tau_2}$, resulting in $1/\tau_1 = 16.7\ s^{-1}$ and $1/\tau_2 = 2.1\ s^{-1}$. F_∞ F at equilibrium and F_1 amd F_2 are amplitudes of the fast and slow components, respectively. F is in volts from a photomultiplier tube. Insets are semilogarithmic representations of data and fits.

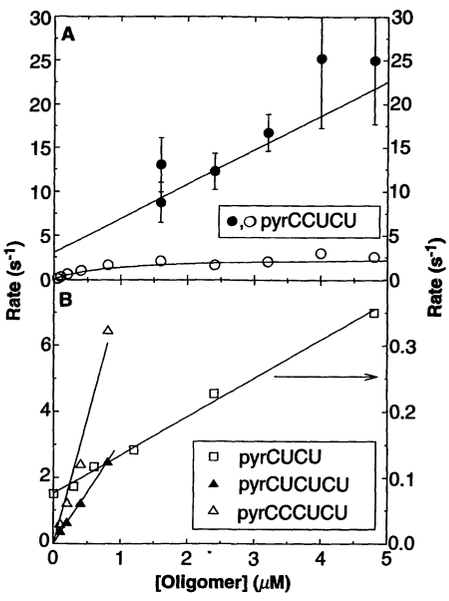

Fig. 3. Dependence of rate on oligomer concentration for binding to L-21 Sca I. Data points come from fits of fluorescence versus time to a single or double exponential as appropriate. Error bars represent standard deviations in $1/\tau_1$ from fits. (**A**) Reaction of 20 nM L-21 Sca I (final concentration) with pyrCCUCU. Line and curve through data points are derived from averages of rate constants determined by direct simulations of traces (Table 1) (*12*). (○) is the slow component of the fluorescence change, $1/\tau_2$; and (●) is the fast component of the fluorescence change, $1/\tau_1$, apparent only at high [pyrCCUCU]. (**B**) Reaction of 40 nM L-21 Sca I (final concentration) with pyrCUCU (□), pyrCUCUCU (▲), or pyrCCCUCU (△). Lines through data points are by linear regression and consistent with simulations.

of k_{-2} was determined by a chase experiment (Table 1).

The first step in Scheme I is base pairing of pyrCCUCU to the IGS. It was modeled by the association of pyrCCUCU with an oligomer mimic for the IGS, GGAGGA. (The true IGS sequence GGAGGG strongly aggregates.) Absorbance melting studies at 280 nm showed a free energy change at 15°C, $\Delta G°_{15}$, of −9.11 kcal/mol for duplex formation, near the −9.17 kcal/mol measured for duplex formation between CCUCU and GGAGGA (Table 2). Evidently, pyr has a minimal effect on the thermodynamics of forming this duplex. For pyrCCUCU association with L-21 Sca I, $-RT\ln(k_1/k_{-1})$ (where R is the gas constant and T is the temperature in Kelvin) provides an estimate of −9.0 kcal/mol for $\Delta G°_{15}$ for the first step (Table 1). Thus, the free energy for forming the intermediate (Scheme I) is similar to that for forming a helix with pyrCCUCU and GGAGGA, consistent with the idea that the first step involves base pairing only.

If the first step in Scheme I involves base pairing only, then the second step must involve formation of the tertiary contacts with P1. For pyrCCUCU, $-RT\ln(k_2/k_{-2})$ provides an estimate of −2.8 kcal/mol for $\Delta G°_{15}$ for the second step (Table 1). Equilibrium dialysis in the presence of 5 mM pdG (2′-deoxyguanosine 5′-monophosphate) suggests that the extra free energy for CUCU binding to L-21 Sca I is approximately −3.8 kcal/mol at 15°C (*6*). Thus, pyrCCUCU retains most of the free energy from tertiary interactions. The difference between pyrCCUCU and CUCU could be due to the inclusion of pdG in the equilibrium dialysis experiments, to the pyr, to the addition of the terminal (non–wild-type) CG pair, or to a combination of these effects. Stopped-flow experiments suggest that inclusion of pdG may contribute ~1 kcal/mol to binding of the 5′ exon mimic.

For pyrCCUCU binding to L-21 Sca I, the four rate constants in Table 1 indicate the overall dissociation constant, K_d, is 1.1 nM (Scheme I). Fluorescence titration with 5 nM L-21 Sca I and 5 to 125 nM pyrCCUCU indicates that $K_d < 5$ nM. (Fluorescence intensity is too weak to allow determinations by titration of $K_d < 5$ nM.) Fluorescence titration with pyrCUCU gives a K_d of 990 nM (*13*). Extrapolating this K_d to pyrCCUCU with the predicted $\Delta G°_{15}$ for the additional CG base pair (*14*), we estimated a K_d of 1.7 nM, consistent with 1.1 nM determined by kinetics. Thus, the two-step mechanism (Scheme I) accounts for all of the binding free energy.

The kinetics of pyrCCUCU and GGAGGA association were measured with stopped-flow fluorescence and absorption ex-

Table 1. Kinetic and thermodynamic parameters for substrate binding to L-21 Sca I at 15°C (Scheme I). All experiments are in 5.0 mM $MgCl_2$, 135 mM NaCl, and 50 mM Hepes (25 mM Na^+) at pH 7.4, unless otherwise noted. L-21 Sca I was prepared and renatured as described (*6*). Stopped-flow experiments were conducted with excitation at 329 nm and emission collected through a band-pass filter centered at 400 nm (*30*). Several shots were averaged for each trace. In all cases, substrate concentration was in excess of L-21 Sca I. Rate constants for pyrCCUCU represent the average of optimal values from direct simulation of each trace, and errors represent SD (*12*).

Substrate	k_1 ($\mu M^{-1}\ s^{-1}$)	k_{-1} (s^{-1})	$-\Delta G°_{15}$ (step 1) (kcal mol^{-1})	k_2 (s^{-1})	k_{-2} (s^{-1})	$-\Delta G°_{15}$ (step 2) (kcal mol^{-1})	$-\Delta G°_{15}$ (total) (kcal mol^{-1})	$-\Delta G°_{15}$ (titration) (kcal mol^{-1})
pyrCUCU	$(0.058\ k_{-1})/k_2$*	$(k_1k_2)/0.058$*	5.4 ± 0.2*	4.7 ± 2*	0.076 ± 0.005†	2.4 ± 0.2	7.8 ± 0.04	7.9 ± 0.08
pyrCCUCU	3.9 ± 0.5	0.5 ± 0.2	9.0 ± 0.2	2.5 ± 0.6	0.02 ± 0.01‡	2.8 ± 0.4	11.8 ± 0.4	>10.9
pyrCUCUCU	3.1 ± 0.05							
pyrCCCUCU	7.6 ± 0.5							

*Because only $k_1(k_2/k_{-1})$ was determined for pyrCUCU, k_2 was calculated with $k_{-1}/k_1 = 80$ μM, as extrapolated from k_{-1}/k_1 for pyrCCUCU and nearest-neighbor parameters for helix propagation (*14*). †We also measured k_2 by mixing 40 nM L-21 Sca I and 1 μM pyrCUCU with a chase of 10 μM CUCU. The decrease in fluorescence fit a single exponential, resulting in a k_{-2} of 0.075 s^{-1}, in good agreement. ‡We measured k_{-2} independently by manually mixing 40 nM L-21 Sca I and 100 nM pyrCCUCU with a chase of 10 μM CCUCU. Values are similar for a 50 μM chase, indicating that dissociation is rate limiting. From Scheme I and $k_{-1} >> k_{-2}$, the observed dissociation rate, k_{off}, is given by $k_{-2}k_{-1}/(k_{-1} + k_2)$. The decrease in fluorescence fit a single exponential, resulting in a k_{off} of $3.0 \times 10^{-3}\ s^{-1}$. The values of k_{-1} and k_2 determined by stopped-flow measurements provide a k_{-2} of 0.02 s^{-1}.

Table 2. Kinetic and thermodynamic parameters for substrate binding to GGAGGA (Fig. 1C). Stopped-flow experiments were performed as in Table 1 but with equal concentrations of pyr oligomer and GGAGGA. Thermodynamics are derived from absorbance versus temperature measurements on oligomers at various total concentrations, C_t. Parameters in the table are derived from plots of $1/T_m$ versus $\log[C_t/4]$ (*14, 31*), where T_m is the temperature at which half the strands are in duplex. Rate constants represent the average of optimal values from simulations (*12*). *T*, temperature; ΔH°, standard enthalpy of duplex formation; ΔS°, standard entropy of duplex formation in entropy units (eu).

Substrate	*T* for kinetics (°C)	k_1 (μM^{-1} s^{-1})	k_{-1} (s^{-1})	$-\Delta G^\circ$ from kinetics (kcal mol^{-1})	$-\Delta G^\circ_{15}$ from melts (kcal mol^{-1})	$-\Delta H^\circ$ from melts (kcal mol^{-1})	$-\Delta S^\circ$ from melts (eu)
pyrCUCU	5	40 ± 3	95 ± 7	7.2 ± 0.06*			
	15	(40)†	(1100)†	(6.0)†			
pyrCCUCU	15	55 ± 5‡	66 ± 1‡,§	9.1 ± 0.1	9.11 ± 0.06‖	44.2 ± 1‖	121.8 ± 3‖
CCUCU					9.17 ± 0.09¶	45.0 ± 1¶	124.3 ± 4¶

*Neglecting pyr, predicted ΔG°_5 in 1M NaCl is −7.3 kcal mol^{-1} (*14*). †We extrapolated values in parentheses to 15°C using nearest-neighbor parameters (*14*) and assuming k_1 for CUCU is temperature independent (*15, 28*). ‡Absorption-detected stopped-flow values at 280 nm for k_1 and k_{-1} are 58 μM^{-1} s^{-1} and 5.7 s^{-1}, respectively. §We also measured k_{-1} by mixing 0.8 μM GGAGGA and 0.8 μM pyrCUCU with a chase of 8 μM CUCU by the stopped-flow technique. The decrease in fluorescence fit a single exponential, resulting in a k_{-1} of 7.7 s^{-1}, in good agreement. ‖Average ΔG°_{15}, ΔH°, and ΔS° derived from fits to melting curves are −9.15 ± 0.2 kcal mol^{-1}, −44.1 ± 3 kcal mol^{-1}, and −121.2 ± 10 eu, respectively. ¶Average ΔG°_{15}, ΔH°, and ΔS° derived from fits to melting curves are −9.51 ± 0.3 kcal mol^{-1}, −49.7 ± 3 kcal mol^{-1}, and −139.6 ± 10 eu, respectively. Predicted ΔG°_{15}, ΔH°, and ΔS° in 1M NaCl are −9.8 kcal mol^{-1}, −51.7 kcal mol^{-1}, and −145.3 eu, respectively (*14*).

periments and are consistent with a one-step bimolecular mechanism (Fig. 1C and Table 2). The K_{-1}'s determined by stopped-flow and absorbance melting agree (Table 2); K_{-1} is the dissociation constant shown in Scheme I. The k_1 is almost four times greater than any reported value for oligonucleotide duplex formation (*15*) although still 100 times slower than rates for diffusion-controlled reactions of multiply charged species (*16*). The k_1 and k_{-1} for this model system are more than tenfold greater than for pyrCCUCU binding to L-21 Sca I. This contrasts with observations for UUCA binding to phenylalanine-specific $tRNA^{Phe}$ (*17*). There, k_1 and k_{-1} are similar for binding to intact tRNA and the excised single-stranded binding site. Perhaps the entrance and exit of pyrCCUCU to the IGS are hindered, many of the encounters between pyrCCUCU and L-21 Sca I do not result in the collision with the IGS required for capture, or both (*18*). Fluorescence amplitudes required for adequate simulation of the data (*12*) indicate that the intermediate in Scheme I is about 3.5 times more fluorescent than the pyrCCUCU-GGAGGA duplex. These differences suggest that P1 in the intermediate is at least partially shielded from solvent and not directly accessible from solution. An understanding of the factors affecting the rate of association may allow engineering of a ribozyme with an association rate as large as for pyrCCUCU + GGAGGA. This would increase discrimination of ribozyme cleavage (*19*).

We further tested the mechanism in Scheme I by binding pyrCUCUCU, pyrCCCUCU, and pyrCUCU to L-21 Sca I. Because tertiary contacts appear limited to the 3′ most UCU (*5, 6, 9*), k_2 and k_{-2} are expected to be similar for these substrates. Also, k_1 should be similar (*20*). Hence, k_{-1} is the only rate constant expected to strongly vary for these substrates.

In the rapid mixing experiments with pyrCCUCU and L-21 Sca I, a single exponential is observed for [pyrCCUCU] ≤ 0.8 μM and a double exponential for [pyrCCUCU] ≥ 1.6 μM (Fig. 2). This is expected from the rates in Scheme I. At [pyrCCUCU] ≤ 0.8 μM, the rate of helix formation with L-21 Sca I, k_1[pyrCCUCU], is slower than or roughly the same as the rate for the conformational change, k_2, and the intermediate does not observably accumulate (*21*). At [pyrCCUCU] ≥ 1.6 μM, the conformational change becomes rate limiting, and the intermediate accumulates, explaining the double exponential. Observation of the intermediate in stopped-flow studies of hexamer binding to L-21 Sca I was difficult because total fluorescence enhancement is reduced by factors of 3 and 5 relative to pyrCCUCU. Nevertheless, at 1.6 μM pyrCUCUCU and 0.2 μM L-21 Sca I, the kinetic trace is unmistakably double exponential. Whereas the signal-to-noise ratio is too low for accurate determination of k_2, an estimate of 1 s^{-1} was obtained, consistent with k_2 for pyrCCUCU (Fig. 1A). For pyrCCCUCU, all kinetic traces with an adequate signal-to-noise ratio fit single exponentials (*22*).

For both hexamers at concentrations ≤0.8 μM, rates obtained from fitting traces to single exponentials are linear with hexamer concentration (Fig. 3B). Additional base pairing in a hexamer makes $k_{-1} << k_2$ (*14, 20*), and Eq. 2 may be reduced to a straight line with slope k_1 and intercept $k_{-1}k_{-2}/k_2$. Extrapolation from pyrCCUCU (*14, 20*) results in predictions of intercepts for pyrCUCUCU and pyrCCCUCU of 4×10^{-4} s^{-1} and 2×10^{-6} s^{-1}, respectively, consistent with the observed intercepts near zero (Fig. 3B). Furthermore, the slopes for the plots for pyrCUCUCU and pyrCCCUCU (Fig. 3B) are similar to the k_1 for pyrCCUCU binding to L-21 Sca I (Table 1) (*20*). Thus, the data for both hexamers binding to L-21 Sca I is consistent with Scheme I. Additionally, k_1 for pyrCCCUCU at 15°C in 5 mM Mg^{2+} is similar to the value of 1.7×10^6 M^{-1} s^{-1} measured for GGCCCUCU by pulse-chase experiments at 50°C in 10 mM Mg^{2+} and a lower Na^+ concentration (*23*).

For pyrCUCU, only single exponentials were observed and are linear with tetramer concentration (Fig. 3B). Reduced base pairing in a tetramer makes $k_{-1} >> (k_2, k_{-2})$ (*14, 20*), and Eq. 2 may be reduced to a straight line with slope $k_1(k_2/k_{-1})$ and intercept k_{-2} (*24*). The intercept in Fig. 3B gives k_{-2} of 0.076 s^{-1} for pyrCUCU, in reasonable agreement with 0.02 s^{-1} for pyrCCUCU (Table 1). Nearest-neighbor extrapolation (*14*) from pyrCCUCU to pyrCUCU predicts K_{-1} = 80 μM, giving k_2 = 4.7 s^{-1} (equivalent to slope × K_{-1}) in reasonable agreement with 2.5 s^{-1} for pyrCCUCU. According to Scheme I, the ratio of intercept to slope in Fig. 3B is K_d. This ratio is 1.3 μM, consistent with the K_d of 0.99 μM obtained by titration (*13*). The minimal mechanism consistent with all the stopped-flow and thermodynamic data for all the substrates is Scheme I (*25*). In this scheme, tertiary interactions form at a rate of about 3 s^{-1}, roughly 1000-fold slower than typical intramolecular secondary structures (*26*).

Two-step binding of substrate to L-21 Sca I has also been inferred from studies of the infidelity of cleavage of RNA and modified substrates by J1/2 mutants of L-21 Sca I (*27*). These studies suggest $k_2 \geq 1333$ s^{-1} at 50°C in 10 mM Mg^{2+}, much larger than the k_2 of 2.5 s^{-1} at 15°C in 5 mM Mg^{2+} reported here for pyrCCUCU. There are many potential origins for this difference. The energetic barrier to uptake of P1 may be ≥33 kcal/mol [the equivalent of breaking three to four average base pairs (*14, 20*)], k_2 may depend on mutations in J1/2 or the L-21 Sca I renaturation protocol, or the two experimental approaches may probe different steps in the mechanism.

There is much to learn about substrate recognition by ribozymes.

REFERENCES AND NOTES

1. R. B. Waring, C. Scazzocchio, T. A. Brown, R. W. Davies, *J. Mol. Biol.* **167**, 595 (1983); M. D. Been and T. R. Cech, *Cell* **47**, 207 (1986).
2. F. X. Sullivan and T. R. Cech, *Cell* **42**, 639 (1985); A. J. Zaug and T. R. Cech, *Science* **231**, 470 (1986).
3. A. J. Zaug, C. A. Grosshans, T. R. Cech, *Biochemistry* **27**, 8924 (1988).
4. N. Sugimoto, M. Tomka, R. Kierzek, P. C. Bevilacqua, D. H. Turner, *Nucleic Acids Res.* **17**, 355 (1989).
5. A. M. Pyle and T. R. Cech, *Nature* **350**, 628 (1991).
6. P. C. Bevilacqua and D. H. Turner, *Biochemistry* **30**, 10632 (1991).
7. R. Kierzek, P. C. Bevilacqua, Y. Li, D. H. Turner, in preparation.
8. The fluorescence intensities of unbound pyrCUCU, pyrCCUCU, and pyrCUCUCU are approximately 0.5, 0.65, and 0.5 that of pyrCCCUCU, respectively. Steady-state fluorescence measurements were performed on a Perkin-Elmer MPF-44A fluorimeter with excitation at 329 nm and emission at 397 nm under the conditions listed in Table 1.
9. S.-H. Kim and T. R. Cech, *Proc. Natl. Acad. Sci. U.S.A.* **84**, 8788 (1987); F. Michel and E. Westhof, *J. Mol. Biol.* **216**, 585 (1990).
10. Reactions were run as described (*6*) except in 5.0 mM $MgCl_2$, 135 mM NaCl, and 50 mM Hepes (25 mM Na^+) at pH 7.4, and reactions were initiated by addition of L-21 Sca I. Reactions went to approximately 90% completion. Formation of the product, p*UCG, was fit to $[p*UCG] = [p*UCG]_{t=\infty}(1 - e^{-k_{obs}t})$, where k_{obs} is the observed rate constant (s^{-1}) and t is time (s). Because [UCGA] << [L-21 Sca I] << K_m^{UCGA} [K_m (Michaelis constant) for UCGA is 55 μM], $k_{obs}/[\text{L-21 Sca I}]_o = k_{cat}/K_m$ for UCGA. The k_{cat}/K_m for cleavage of 10 nM p*UCGA by pyrCUCU, CUCU, pyrCCUCU, CCUCU, and water (50 μM 5′ exon mimic and 5 μM L-21 Sca I) are 120, 120, 220, 130, and 55 M^{-1} s^{-1}, respectively. The k_{cat}/K_m for cleavage of 10 nM p*UCGA by pyrCCUCU, pyrCUCUCU, pyrCCCUCU, and water (0.5 μM 5′ exon mimic and 0.5 μM L-21 Sca I) are 140, 98, 68, and 58 M^{-1} s^{-1}, respectively. The presence of a ribose substrate suppresses the rate of hydrolysis in a related reaction (*4*).
11. K. Johnson, in *The Enzymes*, D. Sigman, Ed. (Academic Press, New York, 1992), vol. 20, pp. 1–61.
12. B. A. Barshop, R. F. Wrenn, C. Frieden, *Anal. Biochem.* **130**, 134 (1983); C. T. Zimmerle and C. Frieden, *Biochem. J.* **258**, 381 (1989).
13. Titration was performed with [L-21 Sca I] held constant at 40 nM; [pyrCUCU] was varied from 0.2 to 2.1 μM. Data were fit by nonlinear least squares to $\Delta F = [\text{pyrCUCU}]/(K_{-1}K_{-2} + [\text{pyrCUCU}])$, where F is fluorescence intensity; $\Delta F \equiv F_{bound}/F_{bound}^{max}$, and $F_{bound} \equiv F_{total} - F_{oligomer}$. Here F_{bound}, F_{bound}^{max}, and $F_{oligomer}$ are, respectively, F due to bound oligomer at any [oligomer], F when all L-21 Sca I is bound to oligomer, and F due to unbound oligomer.
14. S. M. Freier *et al.*, *Proc. Natl. Acad. Sci. U.S.A.* **83**, 9373 (1986); L. He, R. Kierzek, J. SantaLucia, Jr., A. E. Walter, D. H. Turner, *Biochemistry* **30**, 11124 (1991).
15. D. H. Turner, N. Sugimoto, S. M. Freier, in *Nucleic Acids*, vol. 1C of *Landolt-Bornstein Series*, W. Saenger, Ed. (Springer-Verlag, Berlin, 1990), pp. 201–227.
16. M. Eigen and G. G. Hammes, *Adv. Enzymol.* **25**, 1 (1963); C.-T. Lin, W. Böttcher, M. Chou, C. Creutz, N. Sutin, *J. Am. Chem. Soc.* **98**, 6536 (1976).
17. K. Yoon, D. H. Turner, I. Tinoco, Jr., *J. Mol. Biol.* **99**, 507 (1975); ———, F. von der Haar, F. Cramer, *Nucleic Acids Res.* **3**, 2233 (1976).
18. A. M. North, *The Collision Theory of Chemical Reactions in Liquids* (Methuen, London, 1964), chap. 7; K. Hiromi, *Kinetics of Fast Enzyme Reactions* (Kodansha, Tokyo, 1979), pp. 258–259; M. Ben-Nun and R. D. Levine, *J. Phys. Chem.* **96**, 1523 (1992).
19. D. Herschlag, *Proc. Natl. Acad. Sci. U.S.A.* **88**, 6921 (1991).
20. The rate constant k_1 is thought to be limited by formation of a nucleation core of one to three nucleotides and should therefore be relatively independent of length beyond a trimer [J. Wetmur and N. Davidson, *J. Mol. Biol.* **31**, 349 (1968); D. Pörschke and M. Eigen, *ibid.* **62**, 361 (1971); M. E. Craig, D. M. Crothers, P. Doty, *ibid.*, p. 383; D. Pörschke, O. C. Uhlenbeck, F. H. Martin, *Biopolymers* **12**, 1313 (1973); (*15, 28*)]. Thus, increased binding is reflected primarily in a reduced k_{-1}.
21. Fitting of kinetic traces by simulation (*12*) suggests the intermediate for pyrCCUCU has only 60% of the fluorescence enhancement of the final state. Thus, the amplitude of the faster rate representing the intermediate is partially diminished relative to the total amplitude.
22. The rate plot for pyrCCCUCU is linear to at least 6.5 s^{-1}, somewhat greater than the expected asymptote for $1/\tau_2$, $k_2 + k_{-2}$, of 2.5 s^{-1}, on the basis of pyrCCUCU. An increase in k_2 from pyrCCUCU to pyrCCCUCU could cause this effect; this is unlikely, however, because tertiary interactions are confined to CUCU (*5, 6, 9*). Alternatively, because $k_{-1} << (k_2, k_{-2})$ for the hexamers (*14, 20*), if the intermediate and final species have similar fluorescence, Scheme I would be described by the simple rate $1/\tau = k_1[\text{pyrCCCUCU}] + k_{-1}k_{-2}/k_2$. This equation results in linear plots, as observed (Fig. 3B). The pyrCCCUCU has a large unbound fluorescence (*8*) and a small total change in fluorescence, suggesting that pyrCCCUCU may have different relative fluorescence coefficients for the intermediate and final species than pyrCCUCU or pyrCUCUCU.
23. D. Herschlag and T. R. Cech, *Biochemistry* **29**, 10159 (1990).
24. In this model, the faster transient described by Eq. 1 is not observed for pyrCUCU because the intermediate state does not build up because of the high value of K_{-1}.
25. Alternatively, binding of pyrCUCU to L-21 Sca I is also consistent with a one-step bimolecular mechanism with a slow association rate of 5.8×10^4 M^{-1} s^{-1} (*20*). Fluorescence-detected stopped-flow experiments with pyrCUCU and GGAGGA at 5°C (the signal-to-noise ratio was too low to permit a measurement at 15°C) indicate that the oligomers associate with a rate of 4.0×10^7 M^{-1} s^{-1} (Table 2). This is similar to the association rate of 5.5×10^7 M^{-1} s^{-1} for pyrCCUCU and GGAGGA at 15°C (Table 2), as expected because association rates for oligomers with GC pairs typically have low activation energies (*15, 28*). Thus, there is no strong dependence of k_1 on oligomer length for the model systems (*20*). The data for binding to L-21 Sca I, however, require a 70-fold increase in k_1 if the mechanism switches from one to two steps when pyrCUCU is replaced by pyrCCUCU (*29*). Because a large change in k_1 and a change in mechanism are unlikely, we favor Scheme I for pyrCUCU binding to L-21 Sca I.
26. R. C. Yuan, J. A. Steitz, P. B. Moore, D. M. Crothers, *Nucleic Acids Res.* 7, 2399 (1979); D. Labuda, G. Striker, D. Pörschke, *J. Mol. Biol.* **174**, 587 (1984).
27. D. Herschlag, *Biochemistry* **31**, 1386 (1992). J1/2 is the unpaired A_3 stretch joining helix P1 and helix P2.
28. A. P. Williams, C. E. Longfellow, S. M. Freier, R. Kierzek, D. H. Turner, *ibid.* **28**, 4283 (1989).
29. Pulse-chase experiments with 5′ ^{32}P-labeled p*CUCU and L-21 Sca I at 50 mM Mg^{2+} and 50 mM Hepes (25 mM Na^+), pH 7.4, at 15°C give apparent association and dissociation rates similar to those for pyrCUCU in 5 mM Mg^{2+} (P. C. Bevilacqua and D. H. Turner, unpublished results). No trapping was observed at 5 mM Mg^{2+}. However, k_1 is expected weakly to be dependent on $[Mg^{2+}]$ in this range (*28*).
30. K. Johnson, *Methods Enzymol.* **134**, 677 (1986).
31. M. Petersheim and D. H. Turner, *Biochemistry* **22**, 256 (1983).

32. We thank E. Kool, L. Lindahl, E. Phizicky, and K. Yoon for comments on the manuscript. Supported by the Office of Naval Research and NIH grants GM 22939 (to D.H.T.) and GM44613 (to K.A.J.). P.C.B. is a Messersmith Fellow and D.H.T. is a Guggenheim Fellow.

28 May 1992; accepted 1 September 1992

Three-Dimensional Structure of Dimeric Human Recombinant Macrophage Colony-Stimulating Factor

Jayvardhan Pandit, Andrew Bohm, Jarmila Jancarik, Robert Halenbeck, Kirston Koths, Sung-Hou Kim*

Macrophage colony-stimulating factor (M-CSF) triggers the development of cells of the monocyte-macrophage lineage and has a variety of stimulatory effects on mature cells of this class. The biologically active form of M-CSF is a disulfide-linked dimer that activates an intrinsic tyrosine kinase activity on the M-CSF receptor by inducing dimerization of the receptor molecules. The structure of a recombinant human M-CSF dimer, determined at 2.5 angstroms by x-ray crystallography, contains two bundles of four α helices laid end-to-end, with an interchain disulfide bond. Individual monomers of M-CSF show a close structural similarity to the cytokines granulocyte-macrophage colony-stimulating factor and human growth hormone. Both of these cytokines are monomeric in their active form, and their specific receptors lack intrinsic tyrosine kinase activity. The similarity of these structures suggests that the receptor binding determinants for all three cytokines may be similar.

Macrophage colony-stimulating factor (M-CSF) is one of a group of at least 18 glycoproteins, collectively known as hematopoietic growth factors, that regulate the growth and differentiation of blood cells (*1*). Native M-CSF is a 70- to 90-kD homodimer that stimulates proliferation and supports survival and differentiation of cells of the mononuclear phagocyte series (*2*). It also potentiates the ability of mature mononuclear phagocytes to perform their differentiated functions by enhancing their